

SIMULATION OF MICROSEISMIC WAVE PROPAGATION USING HIGH-ORDER FINITE DIFFERENCE VELOCITY IMPLEMENTATION ON BOTH SOURCE AND MEDIA

YI YAO^{1,2,3}, YIBO WANG^{1,2,*}, QINGFENG XUE^{1,2,3} and XU CHANG^{1,2}

¹ Key Laboratory of Shale Gas and Geoengineering, Institute of Geology and Geophysics, Chinese Academy of Sciences, Beijing 100029, P.R. China.

² Institution of Earth Science, Chinese Academy of Sciences, Beijing 100029, P.R.China.
wangyibo@mail.iggcas.ac.cn

³ University of Chinese Academy of Sciences, Beijing 100049, P.R. China.

(Received December 31, 2019; revised version accepted October 5, 2020)

ABSTRACT

Yao, Y., Wang, Y., Xue, Q.F. and Chang, X., 2021. Simulation of microseismic wave propagation using high-order finite difference velocity implementation on both source and media. *Journal of Seismic Exploration*, 30: 45-64.

The characteristics of micro-seismic wave propagation of different source types have raised the interest of seismologists in the past few decades. When using staggered grid finite difference method as simulator, we need to establish a computational staggered grid which has N-th order accuracy and then do source implementation on this grid. There are two kinds of source implementations. One is the stress implementation, which applies the body force onto stress grid directly, and the other is the velocity implementation, which needs to convert body force into velocity component first and then applies the converted velocity component onto velocity grid. The existing velocity implementations mostly do the force-to-velocity conversion based on second-order accuracy, and this kind of implementation is fine when the wave propagation simulator also has second-order accuracy. However, with the increasing accuracy of finite difference simulator, there will be increasing errors due to the calculation order difference between wave propagation simulator and force-to-velocity conversion. We propose a N-th order staggered grid finite difference simulation formula which also has N-th order accuracy of force-to-velocity conversion. We make comparisons with analytical solutions in 3D homogeneous medium, and the results show the effectiveness and high accuracy of proposed approach.

KEY WORDS: microseismic propagation simulation, moment tensor,
high-order velocity implementation, staggered grid finite difference.

INTRODUCTION

Micro-seismic is a seismic wave caused by weak rock fracture. It generally occurs on fault plane of fracture and can be used to study the underground stress condition, as well as the processes of rock rupture (Staněk et al., 2014). Besides, micro-seismic can also depict the change of seismic property in space-time between the source and receiving points. Through the analysis of micro-seismic characteristics, we can study the fracture mechanism of underground cracks and evaluate the effect of hydraulic fracturing (Baig and Urbanic, 2010).

Burridge and Knopoff (1964) proposed the moment tensor theory, which is helpful to study micro-seismic mechanisms. Any types of moment tensors can be decomposed into spherical tensor and deviatoric tensor. The latter part can be further broken down into a variety of forms. Among them, the moment tensor is more inclined to decompose into three components: isotropic (ISO), double-couple (DC), and compensated linear vector dipoles (CLVD).

Generally speaking, an analytical solution is the most accurate method, which can obtain the displacement record by convolution of Green's function with source time function. Some methods are proposed to calculate the Green's function, including DWN (Bouchon, 2003). Even though these methods have a higher computing efficiency, they can hardly be applied to complex medium. The convenience to insert source and the ability to solve complex problems make the numerical techniques stand out.

Varieties of numerical methods that have been developed sufficiently mature, are of importance to seismology for providing abundant information, such as the simulation of wave propagation. The most widely used method in seismic applications is the Finite Difference (FD) method with staggered grids (Madariaga, 1976; Virieux, 1984, 1986; Levander, 1988). One key issue of microseismic wave propagation simulation is how to implement the seismic source into the staggered grid scheme.

Owing to the velocity-stress equations, the source can be added to the stress grid (Coutant et al., 1995) or velocity grid (Yomogida and Etgen, 1993). Graves (1996) proposed the detailed formulas to describe the incorporation of moment tensor sources, and we call it a conventional implementation (CI) method. From these formulas, Li et al. (2015) applied the equations into three basic kinds of moment tensor, obtaining the simulation of wave propagation in the different medium.

In general, to improve the accuracy and minimize the discrepancy, higher order scheme is usually used in simulation. Nevertheless, when it comes to velocity implementation, only the second order spatial form will not introduce discrepancy problem. Therefore, we propose an improved formulation with velocity implementation, which also increases the accuracy.

In this paper, the overview of moment tensor to explain source mechanism will be described firstly. Then the conventional implementation and proposed new implementation with high order spatial form through theoretical analysis are illustrated. Furthermore, we apply the new formulations into the 3D homogeneous elastic medium, obtaining a series of snapshots and records. A comparison with the analytical solution will demonstrate the superiority of the improved method.

A BRIEF OVERVIEW OF MOMENT TENSOR

Moment tensor provides a general theoretical description of seismic sources based on generalized force couple (Fig. 1).

$$M = \begin{bmatrix} M_{xx} & M_{xy} & M_{xz} \\ M_{yx} & M_{yy} & M_{yz} \\ M_{zx} & M_{zy} & M_{zz} \end{bmatrix} . \quad (1)$$

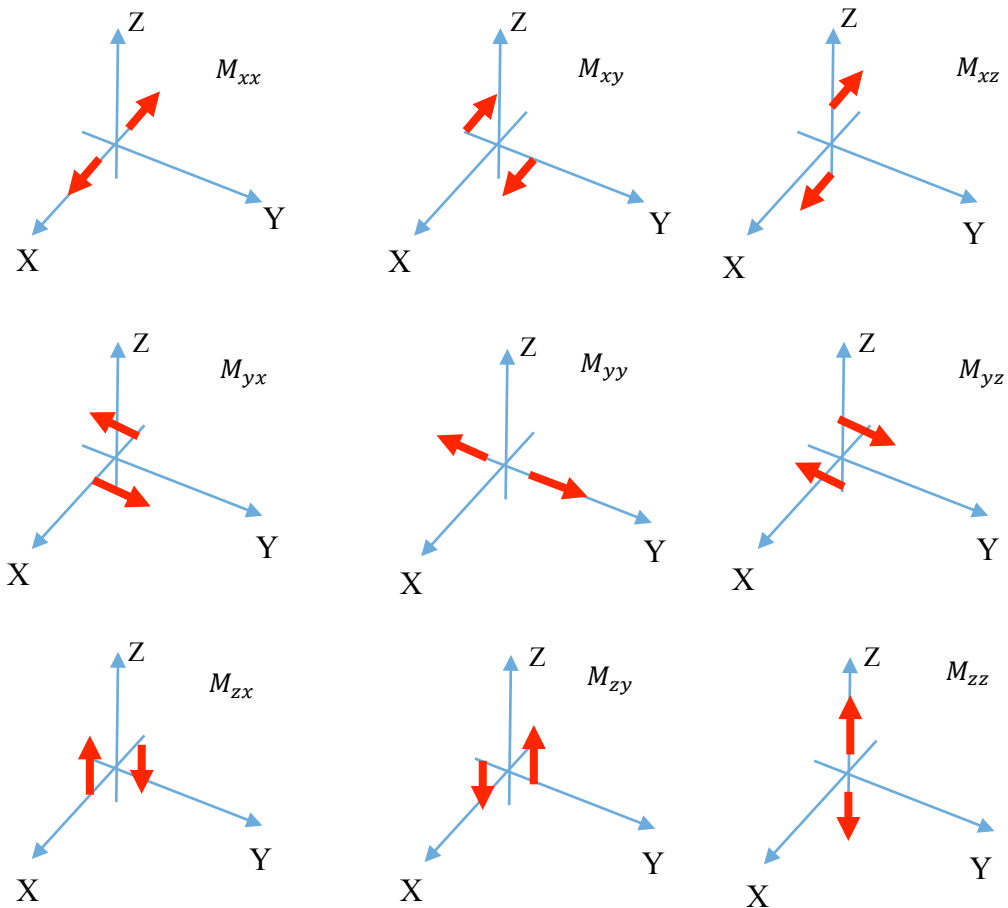


Fig. 1. The nine force couples used for microseismic source description.

Due to the conservation of angular and linear momentum, the seismic moment tensor is symmetrical, meaning that only six of the nine components are independent. The review paper by Jost and Herrmann (1998) has given the overview to the decomposition of moment tensors. There are two possible ways to decompose a full moment tensor, either into an isotropic and deviatoric tensor or into a general mixed-mode shear crack and a residual isotropic component. The deviatoric part can be further decomposed into DC or CLVD primary sources. This paper will adopt the first decomposition mode, as shown in the formulation (2), which can represent the ISO, DC, and CLVD by mathematical form, in sequence. The pure ISO source is a volumetric source and its moment tensor consist of equal-value diagonal elements and zeros for the off-diagonal elements; the DC source is caused by shear faulting; the CLVD source describes that one dipole can be compensated by two other dipoles. Note that the DC and CLVD sources both have no volumetric change because of zero traces of moment tensor.

$$M_{ISO} = \begin{bmatrix} 1 & 0 & 0 \\ 0 & 1 & 0 \\ 0 & 0 & 1 \end{bmatrix} \quad M_{DC} = \begin{bmatrix} 0 & 0 & 1 \\ 0 & 0 & 0 \\ 1 & 0 & 0 \end{bmatrix} \quad M_{CLVD} = \begin{bmatrix} -1 & 0 & 0 \\ 0 & -1 & 0 \\ 0 & 0 & 2 \end{bmatrix} \quad (2)$$

Additionally, it is necessary to understand the relationship between the moment tensor and body forces. According to the equations of Aki and Richards (2002), the equivalent forces yield the following equation.

$$M_{pq} = \iiint_V f_p \eta_q dv \quad . \quad (3)$$

Here f_p means equivalent force, and η_q is the projection displacement.

That is to say, for a small uniform volume, the body force in average can be deduced as follows:

$$f_p = \frac{M_{pq}}{V \cdot d_q} \quad . \quad (4)$$

Here V is the grid volume, d_q is the spatial step.

Conventional implementation schemes on velocity grid

As previously mentioned, plenty of papers illustrate that body forces can be added to the velocity grid. The elastodynamic equations in the homogeneous medium can be described as

$$\rho \frac{\partial v_x}{\partial t} = \frac{\partial \tau_{xx}}{\partial x} + \frac{\partial \tau_{xy}}{\partial y} + \frac{\partial \tau_{xz}}{\partial z} + f_x \quad , \quad (5)$$

$$\rho \frac{\partial V_y}{\partial t} = \frac{\partial \tau_{xy}}{\partial x} + \frac{\partial \tau_{yy}}{\partial y} + \frac{\partial \tau_{yz}}{\partial z} + f_y \quad , \quad (6)$$

$$\rho \frac{\partial V_z}{\partial t} = \frac{\partial \tau_{xz}}{\partial x} + \frac{\partial \tau_{yz}}{\partial y} + \frac{\partial \tau_{zz}}{\partial z} + f_z \quad . \quad (7)$$

Here, (V_x, V_y, V_z) represent the velocity components along x , y and z direction, respectively. $(\tau_{xx}, \tau_{yy}, \tau_{zz}, \tau_{xy}, \tau_{xz}, \tau_{yz})$ are stress-tensor components, ρ is density, and (f_x, f_y, f_z) represent the equivalent forces.

The elastodynamic equations can be solved by the staggered-grid FD method. Fig. 2 shows the discrete layout for staggered-grid used in the forward modeling. The spatial and temporal derivatives of the wavefield components are obtained by:

$$g_f = \frac{\partial f}{\partial x} = \frac{1}{\Delta x} \sum_{n=1}^N c_n [f(x + (n - \frac{1}{2}) \Delta x) - f(x - (n - \frac{1}{2}) \Delta x)] \quad , \quad (8)$$

where c_n is differences coefficients and $2N$ represents the order of FD scheme. Supposed the source locates at the grid point (i, j, k) , the discrete form of the elastodynamic eqs. (5-7) are given by:

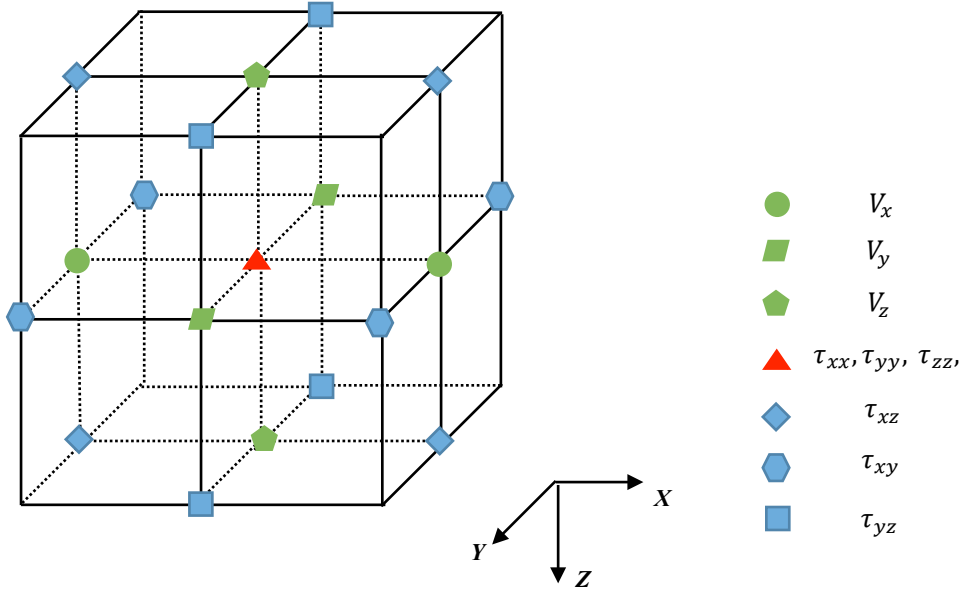


Fig. 2. The computing grid for the finite difference modeling scheme.

$$V_x^{n+\frac{1}{2}}\left(i+\frac{1}{2}, j, k\right) = V_x^{n-\frac{1}{2}}\left(i+\frac{1}{2}, j, k\right) + \frac{dt}{\rho} \left(g(\tau_{xx}, \tau_{xy}, \tau_{xz}) + f_x\right) \quad (9)$$

$$V_y^{n+\frac{1}{2}}\left(i, j+\frac{1}{2}, k\right) = V_y^{n-\frac{1}{2}}\left(i, j+\frac{1}{2}, k\right) + \frac{dt}{\rho} \left(g(\tau_{xy}, \tau_{yy}, \tau_{yz}) + f_y\right) \quad (10)$$

$$V_z^{n+\frac{1}{2}}\left(i, j, k+\frac{1}{2}\right) = V_z^{n-\frac{1}{2}}\left(i, j, k+\frac{1}{2}\right) + \frac{dt}{\rho} \left(g(\tau_{xz}, \tau_{yz}, \tau_{zz}) + f_z\right) \quad (11)$$

where $g(\tau_{xx}, \tau_{xy}, \tau_{xz})$ is a function of the spatial derivatives of $(\tau_{xx}, \tau_{xy}, \tau_{xz})$. dt means the time interval. Shifting the equivalent forces outside of the bracket, the above equations formulate

$$V_x^{n+\frac{1}{2}}\left(i+\frac{1}{2}, j, k\right) = V_x^{n-\frac{1}{2}}\left(i+\frac{1}{2}, j, k\right) + \frac{dt}{\rho} g(\tau_{xx}, \tau_{xy}, \tau_{xz}) + \frac{dt}{\rho} f_x \quad (12)$$

$$V_y^{n+\frac{1}{2}}\left(i, j+\frac{1}{2}, k\right) = V_y^{n-\frac{1}{2}}\left(i, j+\frac{1}{2}, k\right) + \frac{dt}{\rho} g(\tau_{xy}, \tau_{yy}, \tau_{yz}) + \frac{dt}{\rho} f_y \quad (13)$$

$$V_z^{n+\frac{1}{2}}\left(i, j, k+\frac{1}{2}\right) = V_z^{n-\frac{1}{2}}\left(i, j, k+\frac{1}{2}\right) + \frac{dt}{\rho} g(\tau_{xz}, \tau_{yz}, \tau_{zz}) + \frac{dt}{\rho} f_z \quad (14)$$

Therefore, the variations of velocity components due to the body force are:

$$\Delta V_x\left(i+\frac{1}{2}, j, k\right) = \frac{dt}{\rho} f_x \quad (15)$$

$$\Delta V_y\left(i, j+\frac{1}{2}, k\right) = \frac{dt}{\rho} f_y \quad (16)$$

$$\Delta V_z\left(i, j, k+\frac{1}{2}\right) = \frac{dt}{\rho} f_z \quad (17)$$

And these eqs. (15-17) are adopted as the final velocity implementation form. Given that our research focuses on the microseismic, the source form should be moment tensor. Each of element of moment tensor means a couple of forces, armed in the coordinate direction. In other words, two forces with the same value but the opposite direction should be assigned at two adjacent grid points. Take the M_{xx} as an example, the velocity implementation forms are described as:

$$\Delta V_x\left(i+\frac{1}{2}, j, k\right) = \frac{dt}{\rho} f_x \quad (18)$$

$$\Delta V_x\left(i-\frac{1}{2}, j, k\right) = -\frac{dt}{\rho} f_x \quad (19)$$

We can also derive the implementation of an off-diagonal part similarly.

For example, the application of M_{xz} is given by eqs. (20, 21) and M_{zx} by eqs. (22, 23), respectively.

$$\Delta V_x \left(i + \frac{1}{2}, j, k \right) = -\frac{dt}{\rho} f_x \quad , \quad (20)$$

$$\Delta V_x \left(i + \frac{1}{2}, j, k + 1 \right) = \frac{dt}{\rho} f_x \quad , \quad (21)$$

$$\Delta V_z \left(i, j, k + \frac{1}{2} \right) = -\frac{dt}{\rho} f_z \quad , \quad (22)$$

$$\Delta V_z \left(i + 1, j, k + \frac{1}{2} \right) = \frac{dt}{\rho} f_z \quad . \quad (23)$$

The other components can be deduced in a similar way. Fig. 3 shows how the velocity is added at grid point around the adjacent points with three kinds of the source by the conventional implementation methods.

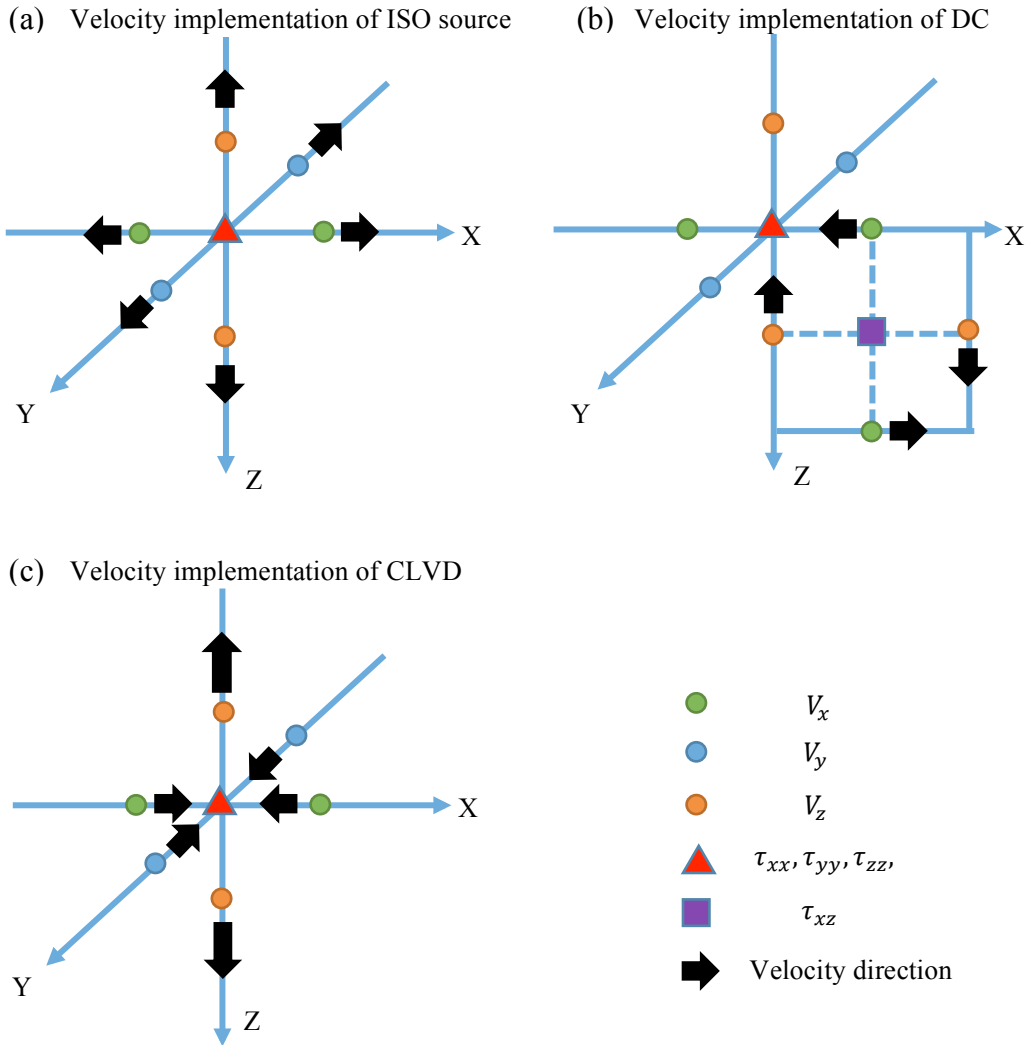


Fig. 3. The sketch map of conventional implementation on velocity grid. (a) ISO sources as an explosive source. (b) DC source of share force on the x-z plane. (c) CLVD sources with no volumetric change.

Higher order implementation schemes on velocity grid

As mentioned in the last part, current implementation can be finished as long as we apply the velocity components into the adjacent points of the source and nothing should be done for other positions. When discretize the elastodynamic equations in (9-11), the function g can take the 2N spatial scheme to improve the numerical accuracy.

It seems that equivalent forces have no relations with the calculations of function g . But it should be noted that the velocity components at this time will be used to calculate the stress components at the next time, which illustrate that the body force mixes into the stress components. Besides, stress implementation method, which adds the force to the stress components, has been validated by many scholars. It also reflects the body force cannot be ignored. So, when taking high order spatial forms, we need to convert body force into velocity component.

Similarly, we assume the source grid point is (i, j, k) , and take the fourth spatial order scheme for easily understood. Referring to the stress implementation method, we make the body force f integrate into stress.

$$\tau'_{xx}(i, j, k) = \tau_{xx}(i, j, k) - f_x \cdot \Delta x \quad (24)$$

Then the change of velocity components can be calculated by:

$$\Delta V_x \left(i + \frac{1}{2}, j, k \right) = \frac{dt}{\rho} (g'_{\tau_{xx}} + g_{\tau_{xy}} + g_{\tau_{xz}}) \quad . \quad (25)$$

The $g'_{\tau_{xx}}$ comprises of force f , and we make the following notation.

$$g_f^n = \frac{1}{\Delta x} [f \left(x + \left(n - \frac{1}{2} \right) \Delta x \right) - f \left(x - \left(n - \frac{1}{2} \right) \Delta x \right)] \quad . \quad (26)$$

Therefore, under the fourth order spatial form condition

$$g'_{\tau_{xx}} = c_1 g_{\tau_{xx}}^{1'} + c_2 g_{\tau_{xx}}^{2'} \quad . \quad (27)$$

And we can get

$$g_{\tau_{xx}}^{1'} \left(i + \frac{1}{2}, j, k \right) = \frac{1}{\Delta x} [\tau_{xx}(i + 1, j, k) - \tau'_{xx}(i, j, k)] \quad (28)$$

$$g_{\tau_{xx}}^{2'} \left(i + \frac{3}{2}, j, k \right) = \frac{1}{\Delta x} [\tau_{xx}(i + 3, j, k) - \tau'_{xx}(i, j, k)] \quad . \quad (29)$$

Place eq. (24) into (28-29), and we can obtain the following equation

$$g_{\tau_{xx}}^{1'} \left(i + \frac{1}{2}, j, k \right) = g_{\tau_{xx}}^1 \left(i + \frac{1}{2}, j, k \right) + f_x \quad (30)$$

$$g_{\tau_{xx}}^{2'} \left(i + \frac{3}{2}, j, k \right) = g_{\tau_{xx}}^2 \left(i + \frac{3}{2}, j, k \right) + f_x \quad . \quad (31)$$

Place eq. (30) back to eqs. (27) and (25), Thus

$$\Delta V_x \left(i + \frac{1}{2}, j, k \right) = \frac{dt}{\rho} \left(g_{\tau_{xx}} + g_{\tau_{xy}} + g_{\tau_{xz}} \right) + \frac{dt}{\rho} \cdot c_1 \cdot f_x \quad (32)$$

Similarly,

$$\Delta V_x \left(i + \frac{3}{2}, j, k \right) = \frac{dt}{\rho} \left(g_{\tau_{xx}} + g_{\tau_{xy}} + g_{\tau_{xz}} \right) + \frac{dt}{\rho} \cdot c_2 \cdot f_x \quad (33)$$

$$\Delta V_x \left(i - \frac{1}{2}, j, k \right) = \frac{dt}{\rho} \left(g_{\tau_{xx}} + g_{\tau_{xy}} + g_{\tau_{xz}} \right) - \frac{dt}{\rho} \cdot c_1 \cdot f_x \quad (34)$$

$$\Delta V_x \left(i - \frac{3}{2}, j, k \right) = \frac{dt}{\rho} \left(g_{\tau_{xx}} + g_{\tau_{xy}} + g_{\tau_{xz}} \right) - \frac{dt}{\rho} \cdot c_2 \cdot f_x \quad (35)$$

In eqs. (28) and (29), we can find that the calculation of the velocity at the point $(i+1/2, j, k)$ and point $(i+3/2, j, k)$ both rely on the body force f . That is the reason why we should make these two velocity grid points get accelerated. It is noted that eq. (24) is for the convenience of our new method description, but not the actual stress implementation for body force f . If the stress implementation wants to be equivalent to the velocity implementation, then the body force f should be changed to the derivative [eq. (36)] or the stress components does not need to be accumulated [eq. (37)].

$$\tau'_{xx}(i, j, k) = \tau_{xx}(i, j, k) - \dot{f}_x \cdot \Delta x \quad (36)$$

$$\tau'_{xx}(i, j, k) = -f_x \cdot \Delta x \quad (37)$$

Fig. 4(a) shows the sketch map of velocity implementation in the x -direction by conventional velocity implementation method.

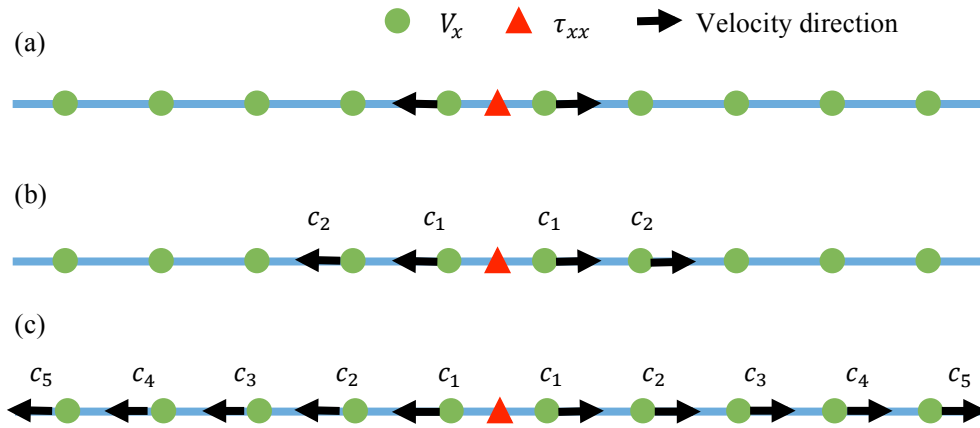


Fig. 4. The sketch map of velocity implementation in the X direction. (a) second order spatial scheme and it indicates only two adjacent points will get accelerated, which is used in the conventional method, regardless of the spatial order scheme; (b) taking fourth order spatial scheme as an example, the higher implementation method requires the equivalent grid points should be get accelerated corresponding to the spatial order scheme, namely the 4-th order force-to-velocity conversion; (c) tenth order spatial scheme. The parameters $(c_1, c_2, c_3, c_4, c_5)$ are the differences coefficients.

In contrast, Fig. 4(b) explains how to accelerate the velocity components by the new approach under the fourth-order spatial scheme. We can conclude that 4-th order staggered grid finite difference simulation should have 4-th order accuracy of force-to-velocity conversion. In our example, the fourth order spatial form will accelerate four velocity points. Likewise, ten velocity grid components should be got accelerated corresponding with tenth order spatial scheme [shown in Fig. 4(c)]. More velocity implementation equations of three basic types of sources with $2N$ order spatial scheme will be given in a similar way. Here, we present the expressions for the distribution of body forces caused by a moment tensor source under the high order spatial scheme. They can be derived from a similar manner as the x dimensional component. And combining with the relation (4), these equations are shown in (38) - (40).

ISO

$$\begin{aligned}
\Delta Vx_{i+1/2+l,j,k} &= c_{l+1} \cdot \frac{Mxx \cdot dt}{\rho \cdot dx \cdot V} (l = 0, \dots, N-1) \\
\Delta Vx_{i+1/2+l,j,k} &= -c_{-l} \cdot \frac{Mxx \cdot dt}{\rho \cdot dx \cdot V} (l = -N, \dots, -1) \\
\Delta Vy_{i,j+1/2+l,k} &= c_{l+1} \cdot \frac{Myy \cdot dt}{\rho \cdot dy \cdot V} (l = 0, \dots, N-1) \\
\Delta Vy_{i,j+1/2+l,k} &= -c_{-l} \cdot \frac{Myy \cdot dt}{\rho \cdot dy \cdot V} (l = -N, \dots, -1) \\
\Delta Vz_{i,j,k+1/2+l} &= c_{l+1} \cdot \frac{Mzz \cdot dt}{\rho \cdot dz \cdot V} (l = 0, \dots, N-1) \\
\Delta Vz_{i,j,k+1/2+l} &= -c_{-l} \cdot \frac{Mzz \cdot dt}{\rho \cdot dz \cdot V} (l = -N, \dots, -1)
\end{aligned} \tag{38}$$

DC

$$\begin{aligned}
\Delta Vx_{i+1/2,j,k+1+l} &= c_{l+1} \cdot \frac{Mxz \cdot dt}{\rho \cdot dx \cdot V} (l = 0, \dots, N-1) \\
\Delta Vx_{i+1/2,j,k+1+l} &= -c_{-l} \cdot \frac{Mxz \cdot dt}{\rho \cdot dx \cdot V} (l = -N, \dots, -1) \\
\Delta Vz_{i+1+l,j,k+1/2} &= c_{l+1} \cdot \frac{Mxz \cdot dt}{\rho \cdot dz \cdot V} (l = 0, \dots, N-1) \\
\Delta Vz_{i+1+l,j,k+1/2} &= -c_{-l} \cdot \frac{Mxz \cdot dt}{\rho \cdot dz \cdot V} (l = -N, \dots, -1)
\end{aligned} \tag{39}$$

CLVD

$$\begin{aligned}
\Delta Vx_{i+1/2+l,j,k} &= -c_{l+1} \cdot \frac{Mxx \cdot dt}{\rho \cdot dx \cdot V} (l = 0, \dots, N-1) \\
\Delta Vx_{i+1/2+l,j,k} &= c_{-l} \cdot \frac{Mxx \cdot dt}{\rho \cdot dx \cdot V} (l = -N, \dots, -1) \\
\Delta Vy_{i,j+1/2+l,k} &= -c_{l+1} \cdot \frac{Myy \cdot dt}{\rho \cdot dy \cdot V} (l = 0, \dots, N-1) \\
\Delta Vy_{i,j+1/2+l,k} &= c_{-l} \cdot \frac{Myy \cdot dt}{\rho \cdot dy \cdot V} (l = -N, \dots, -1) \\
\Delta Vz_{i,j,k+1/2+l} &= 2 \cdot c_{l+1} \cdot \frac{Mzz \cdot dt}{\rho \cdot dz \cdot V} (l = 0, \dots, N-1) \\
\Delta Vz_{i,j,k+1/2+l} &= -2 \cdot c_{-l} \cdot \frac{Mzz \cdot dt}{\rho \cdot dz \cdot V} (l = -N, \dots, -1)
\end{aligned} \tag{40}$$

Comparison with Analytical solution

We compare the solutions obtained by the finite difference method in an elastic, homogeneous infinite media. The parameters used in simulation are $V_p = 3000$ m/s, $V_s = 1731$ m/s, grid spacing - 2 m, and time step - 0.05 ms. The model size is $800 \text{ m} \times 800 \text{ m} \times 800 \text{ m}$. The source locates at the center of the model, whose time function is Ricker wavelet with a central frequency of 100 Hz. The geometry model is depicted in Fig. 5. There is one receiver located at (450 m, 470 m, 510 m). The displacement from a general moment tensor M_{pq} in a homogeneous whole space is:

$$\begin{aligned}
u_i(r, t) &= \frac{1}{4\pi r^4} (15\gamma_i\gamma_p\gamma_q - 3\gamma_i\delta_{pq} - 6\gamma_p\delta_{iq}) \int_{\frac{r}{\alpha}}^{\frac{r}{\beta}} \tau M_{pq}(t - \tau) d\tau \\
&+ \frac{1}{4\pi\alpha^2 r^2} (6\gamma_i\gamma_p\gamma_q - \gamma_i\delta_{pq} - 2\gamma_p\delta_{iq}) M_{pq} \left(t - \frac{r}{\alpha} \right) \\
&- \frac{1}{4\pi\beta^2 r^2} (6\gamma_i\gamma_p\gamma_q - \gamma_i\delta_{pq} - 3\gamma_p\delta_{iq}) M_{pq} \left(t - \frac{r}{\beta} \right) \\
&+ \frac{1}{4\pi\alpha^3 r} (\gamma_i\gamma_p\gamma_q) \dot{M}_{pq} \left(t - \frac{r}{\alpha} \right) + \frac{1}{4\pi\beta^3 r} (\delta_{ip} - \gamma_i\gamma_q) \dot{M}_{pq} \left(t - \frac{r}{\beta} \right)
\end{aligned} \tag{41}$$

The displacement consists of the near-field, intermediate-field, and the far-field term. Before starting the simulation, it is necessary to demonstrate that the conventional method exactly exists discrepancy problem, which is caused by the incompatibility of the general scheme with high order formulation. The ISO source will be the best choice for observing whether the method exists discrepancy problem because it will not produce S-waves

in the homogeneous media and the error will be found easily. Fig. 6 shows the comparison of the simulation record resulting from the conventional method for different orders schemes. It is easily found that discrepancy does not appear in the 2nd order calculations and starts to appear in the 4th order simulations. However, it should be noted that 2nd order results deviate from the others simulations and that's why we get rid of it in the following comparisons. From Fig. 7, the comparisons among conventional numerical results, new proposed results and analytical solution with different spatial orders turn out that as the order continues to increase, the discrepancy error from the traditional method will get arise too. The reason is that the degree of mismatch between source and medium discretization generally increase. We also find that the error from the new method is tailing off. On the basis of these results, all kind of typical sources, including ISO, DC, and CLVD, are tested by the two methods. Considering the accuracy, the tenth spatial order scheme is used in our simulations.

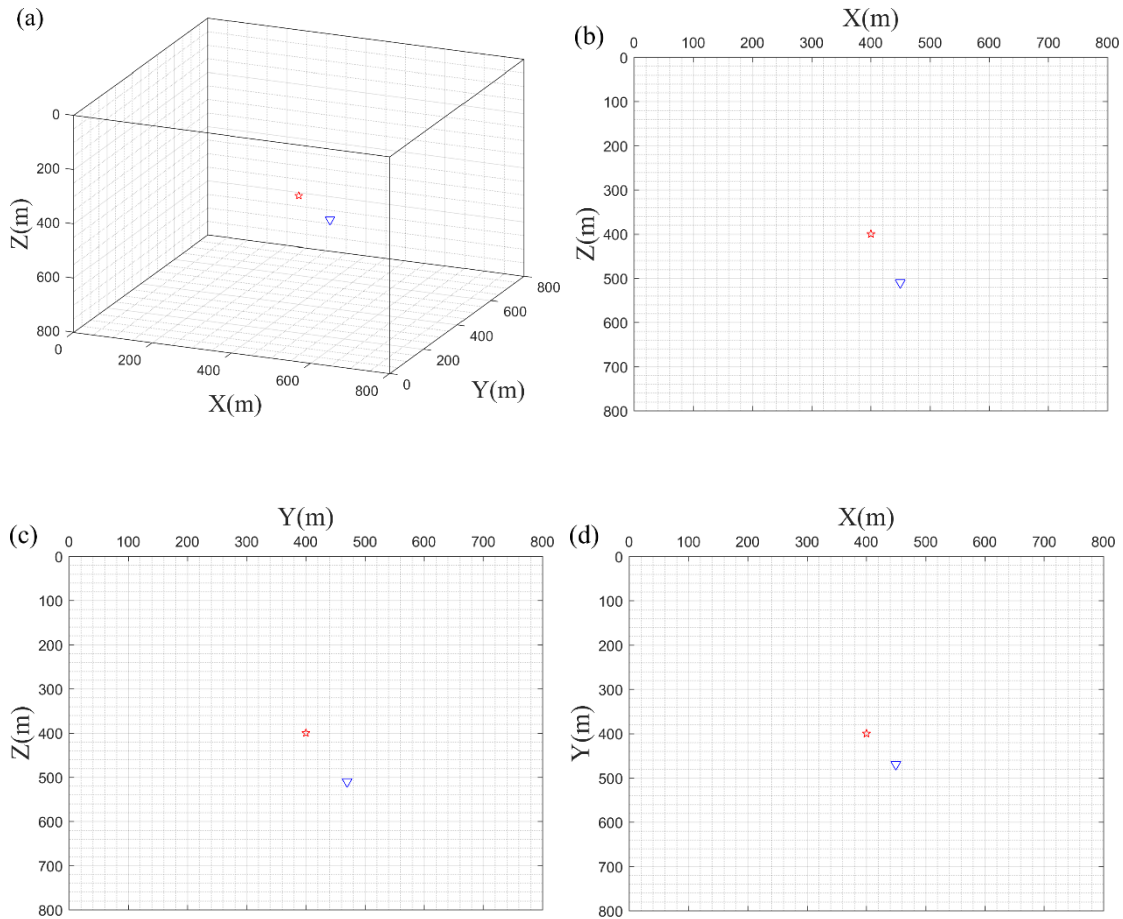


Fig. 5. (a) The source-receiver configuration used for FDM computation. The red star represents microseismic source, the blue triangle means receiver. The microseismic source is placed in the middle of the model. (b-d) Projection of the source and receiver on surface XZ, YZ, XY, sequentially.

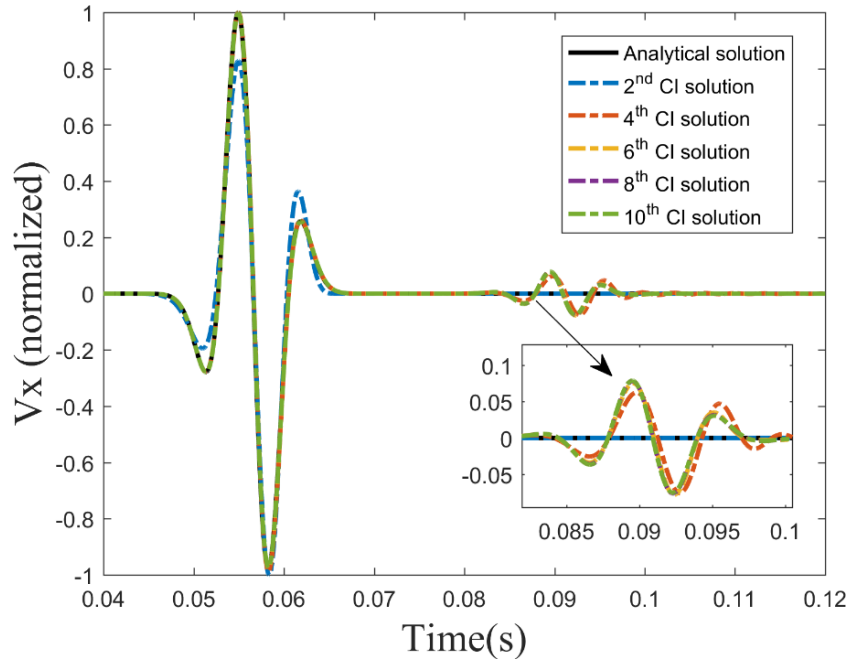


Fig. 6. Comparison of seismic wave generated by ISO source between the analytical solution and the simulated records resulting from the conventional implementation (CI) scheme for different orders.

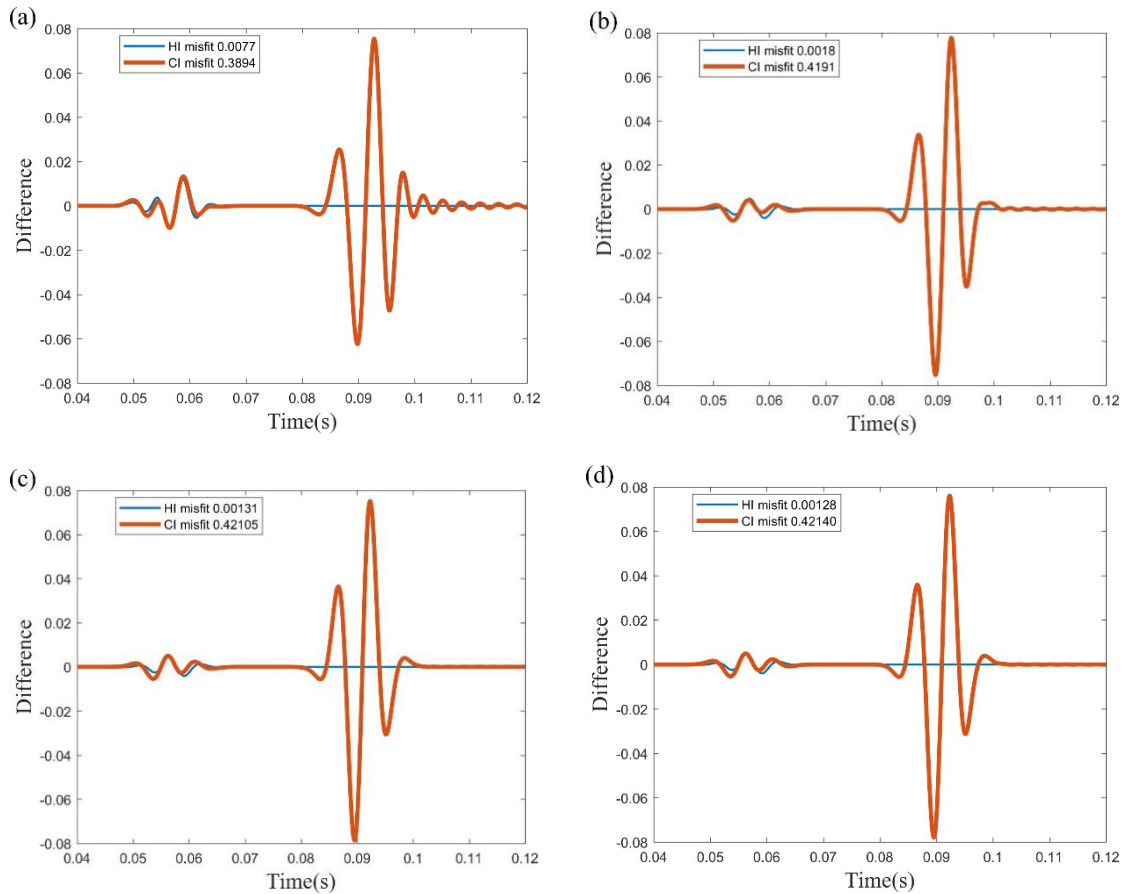


Fig. 7. The differences of conventional solution and new solution from an analytical solution with (a) 4th order; (b) 6th order; (c) 8th order; (d) 10th order spatial discrete scheme. CI means the conventional implementation and HI represents the higher implementation.

ISO

Fig. 8 shows the snapshots of the velocity components computed by the conventional method and the improved method in homogeneous model corresponding to the ISO source. In these diagrams, the snapshots in Fig. 8a contain not only P-waves but also waves of other forms, which are not expected. In contrast, Fig. 8b demonstrates a pure P-wave and is also in accordance with spherical moment tensor, only reflecting in volume change. In addition, we compare the solutions obtained by the numerical method, including conventional velocity implementation and new improved implementation, with exact solutions computed analytically. Figs. 9a, 9c, and 9e represent the microseismic waveforms of X, Y and Z components obtained from two numerical solutions and analytic solution, respectively. These curves are both normalized by their own maximum amplitude, which indicates the magnifying factors of X, Y and Z components. From these figures, two numerical solutions can basically match with the analytical solution. However, it's apparently found that the conventional solutions (red dashed line) hold some residual records. To recognize them clearly, the quantitative differences are calculated through making the numerical solutions minus the analytical solution, and thus we can tell their difference. Figs. 9b, 9d, and 9f present the residuals of the two numerical schemes in X, Y, and Z direction, and the value of misfit equals the residual sum of square (RSS). The value of CI (Conventional Implementation) is larger than HI (Higher Implementation), which means new proposed method will reach a higher precision.

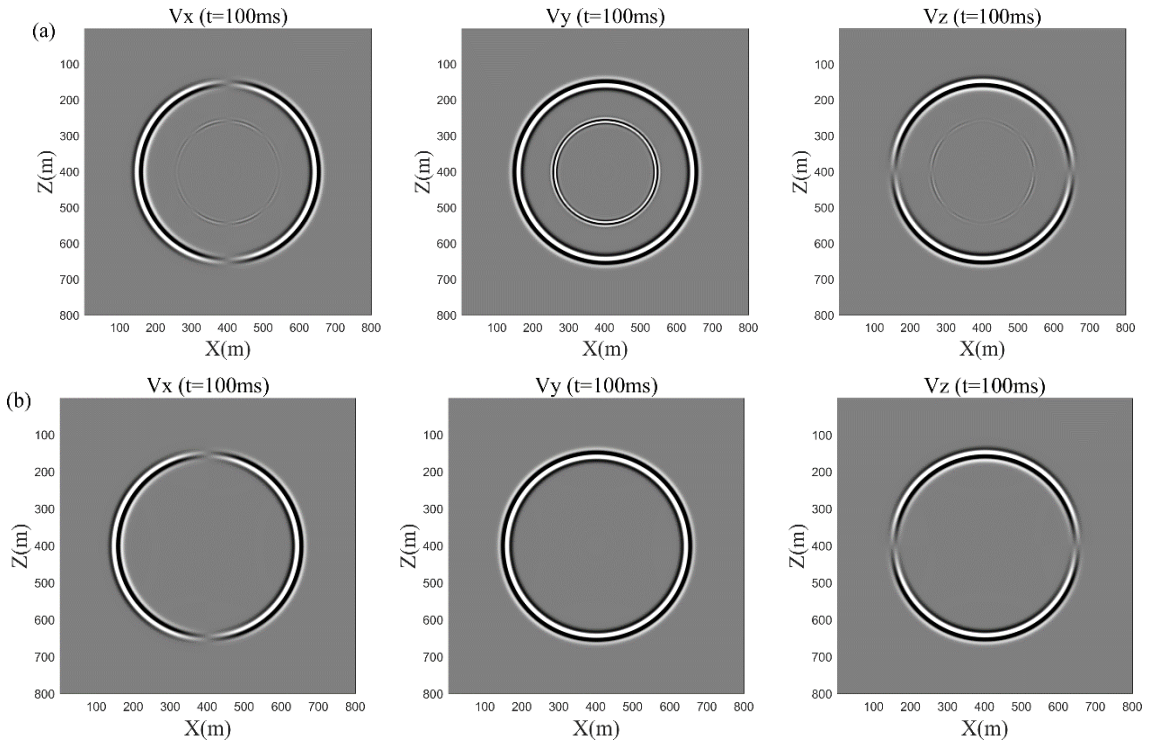


Fig. 8. The seismic snapshots of ISO source computed by (a) conventional velocity implementation; (b) higher velocity implementation with 10th order spatial discrete scheme. From left to right is velocity component of X, Y, and Z, sequentially.

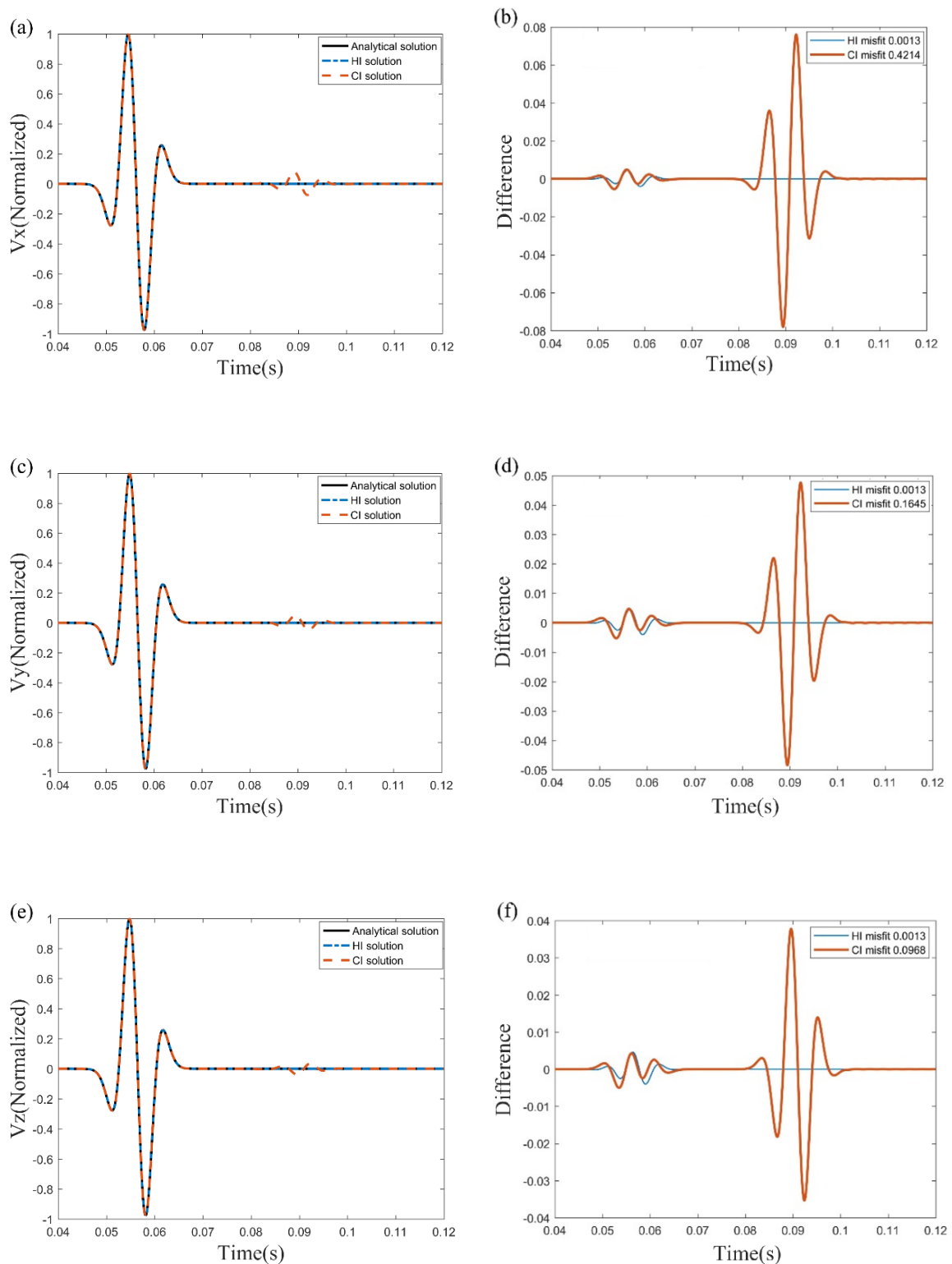


Fig. 9. The normalized velocity component obtained from two numerical solutions with 10-th order spatial discrete and analytic solution are shown in the left column, and their differences are shown in the right column. The source type is same as Fig. 9. From top to bottom is velocity component of X, Y, and Z, sequentially.

DC

We deal with this source in the same way as that in ISO source. Snapshots in Figs. 10a and 10b have barely noticeable difference. At the same time, the Figs. 11a, 11c and 11e also show both the conventional method and the new improved method can solve this situation since two numerical solutions fit the exact solutions very well. And now, the misfits play an essential role, because Figs. 11b, 11d and 11f reveal the proposed method (HI, blue dotted line) is closest to the real value and make it stand out. The reason why snapshots of two methods are almost the same is DC source can generate both P- and S-waves, and the S-wave has intense energy which covers the errors. In contrast, ISO source only produces P-waves in the homogeneous medium, thus the error, no matter how small, will be visible. In conclusion, the two methods can settle down the DC sources, but the new proposed method has higher accuracy.

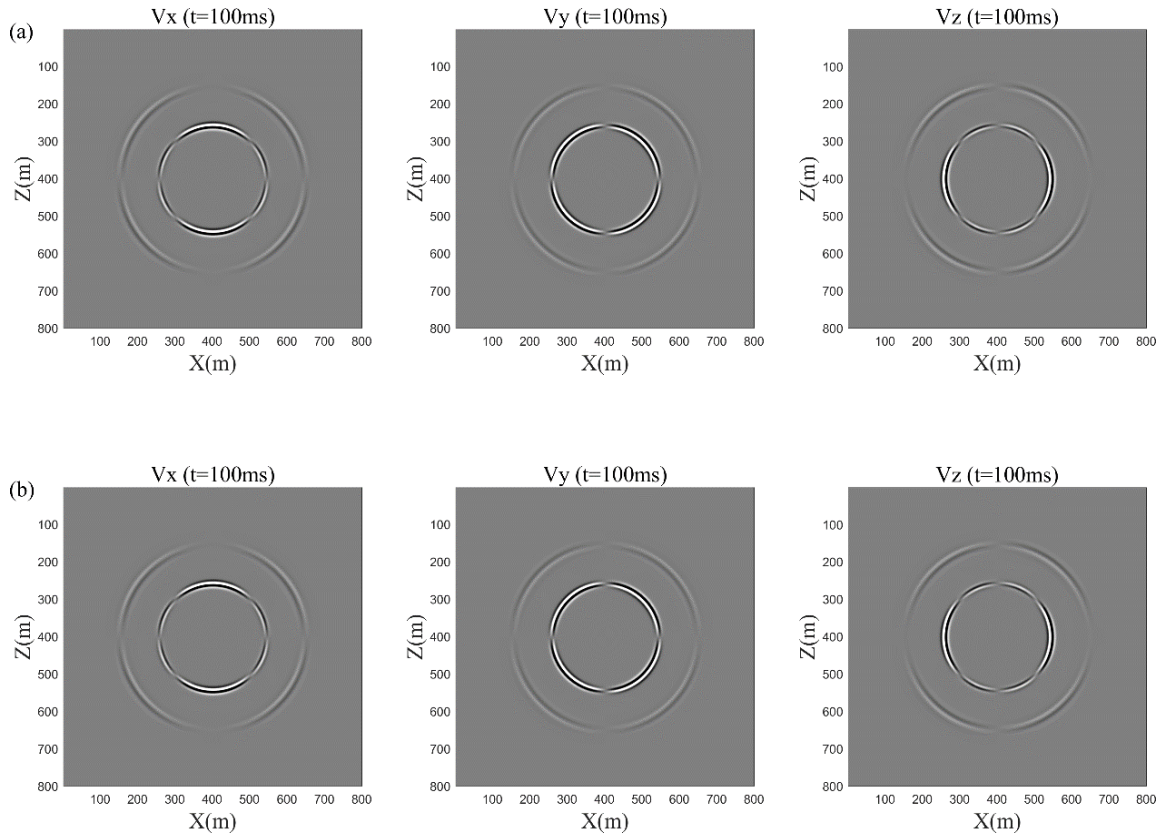


Fig. 10. The seismic snapshots of DC source computed by (a) conventional velocity implementation; (b) higher velocity implementation with 10-th order spatial discrete scheme. From left to right is velocity components of X, Y, and Z, sequentially.

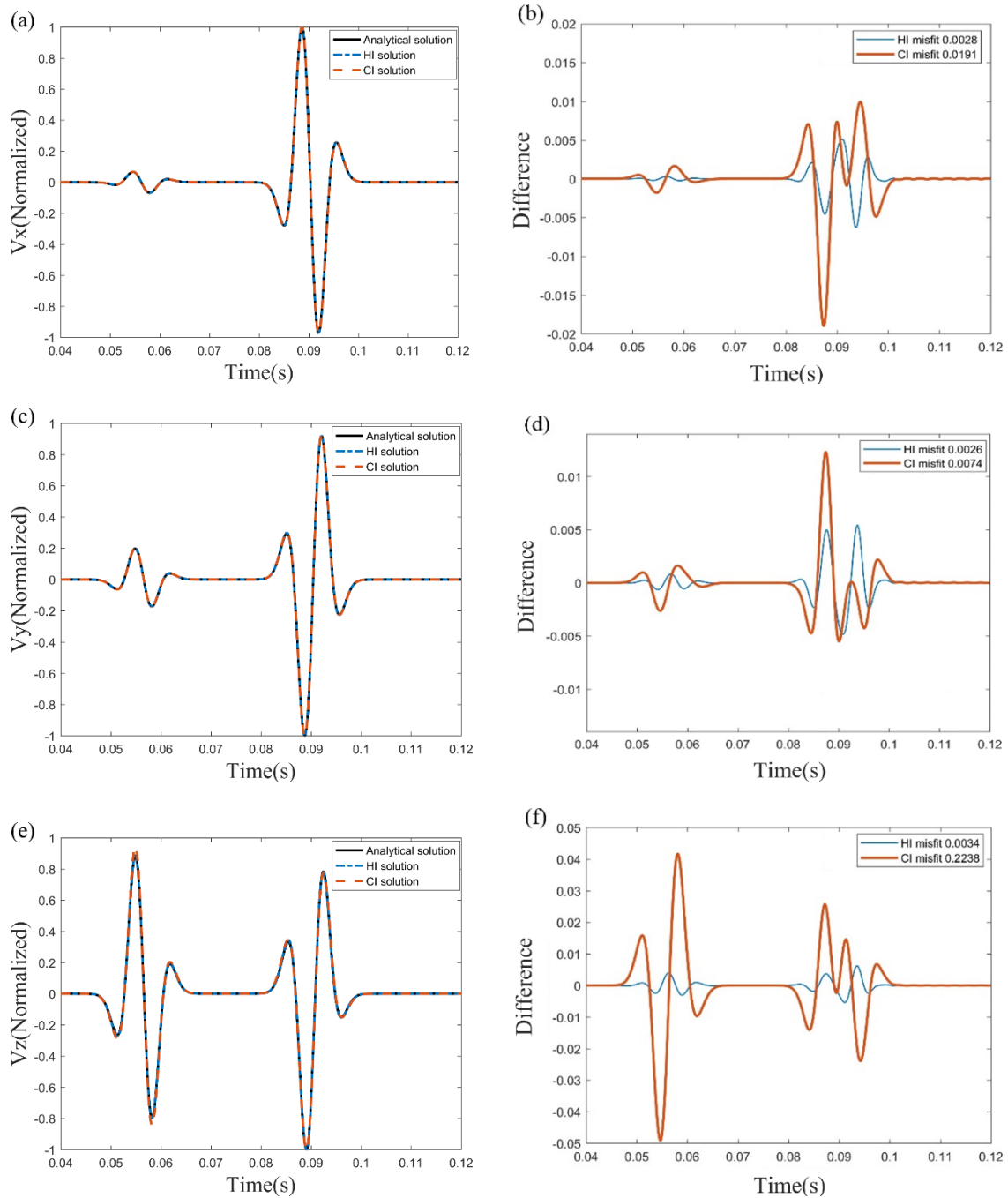


Fig. 11. The normalized velocity component obtained from two numerical solutions with 10th order spatial discrete and analytic solution are shown in the left column, and their differences are shown in the right column. The source type is same as Fig. 11. From top to bottom is velocity component of X, Y, and Z, sequentially.

CLVD

The CLVD source is more similar to the DC source since their moment tensors have the same trace and both they generate P- and S-waves. Therefore, there is no doubt that their result is analogous. Similarity, it is hard to tell the difference in snapshots between the Figs. 12a and 12b, as a result of the relatively small misfit. From Figs. 13a, 13c and 13e, we can

recognize that both the conventional solution represented by the red dashed line and higher new solution represented by a blue dotted line, fit the exact solution well. And Figs. 13b, 13d and 13f demonstrate the same conclusion, that the new improved method will obtain a better solution.

In short, both of the two methods can stimulate different source mechanism but the new improved method is more accurate.

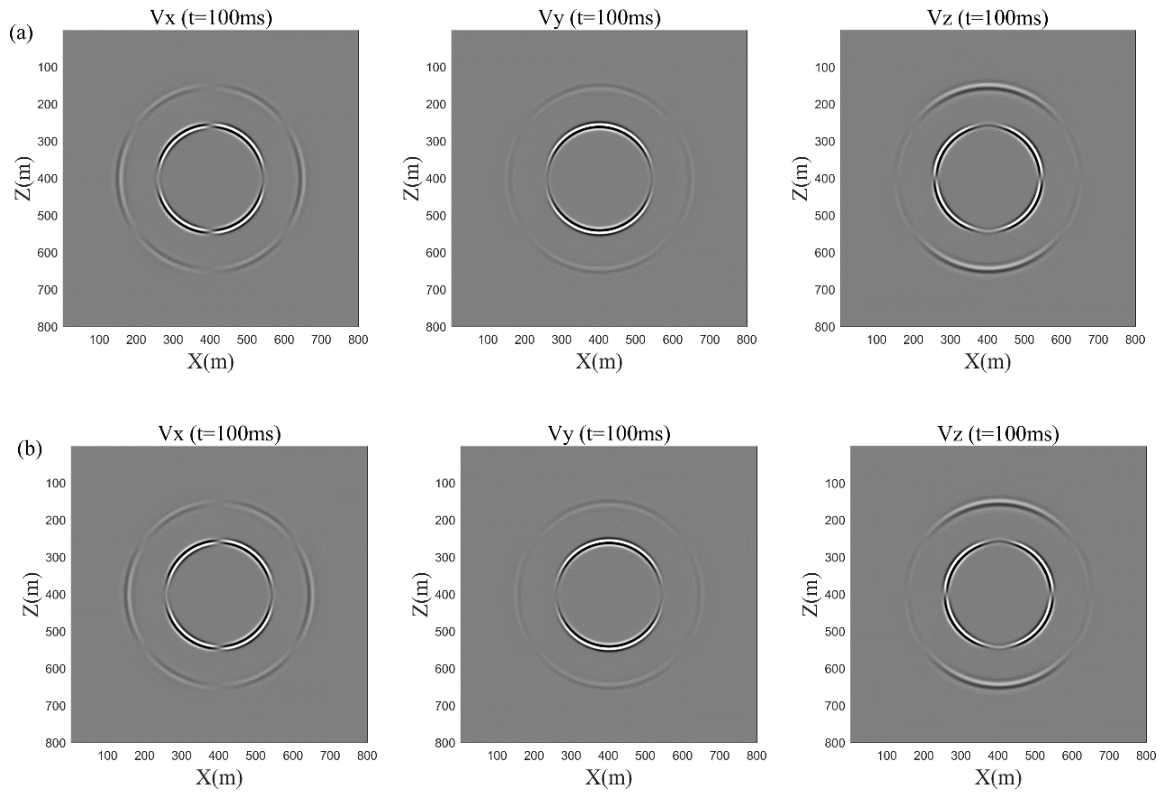


Fig. 12. The seismic snapshots of CLVD source computed by (a) conventional velocity implementation; (b) higher velocity implementation with 10-th order spatial discrete scheme. From left to right is velocity components of X, Y, and Z, sequentially.

CONCLUSIONS

This paper proposes an improved formula to simulate the wave propagation of a seismic source, by representation of moment tensor. And thus, we can obtain more accurate simulation of ISO, DC, CLVD sources in an elastic homogenous infinite media. From the snapshots and synthetic seismogram, we can make the following conclusions.

The kernel of a higher velocity implementation is that a N-th order staggered grid finite difference simulation should have N-th order accuracy of force-to-velocity conversion. It is also the most important difference from the conventional velocity implementation.

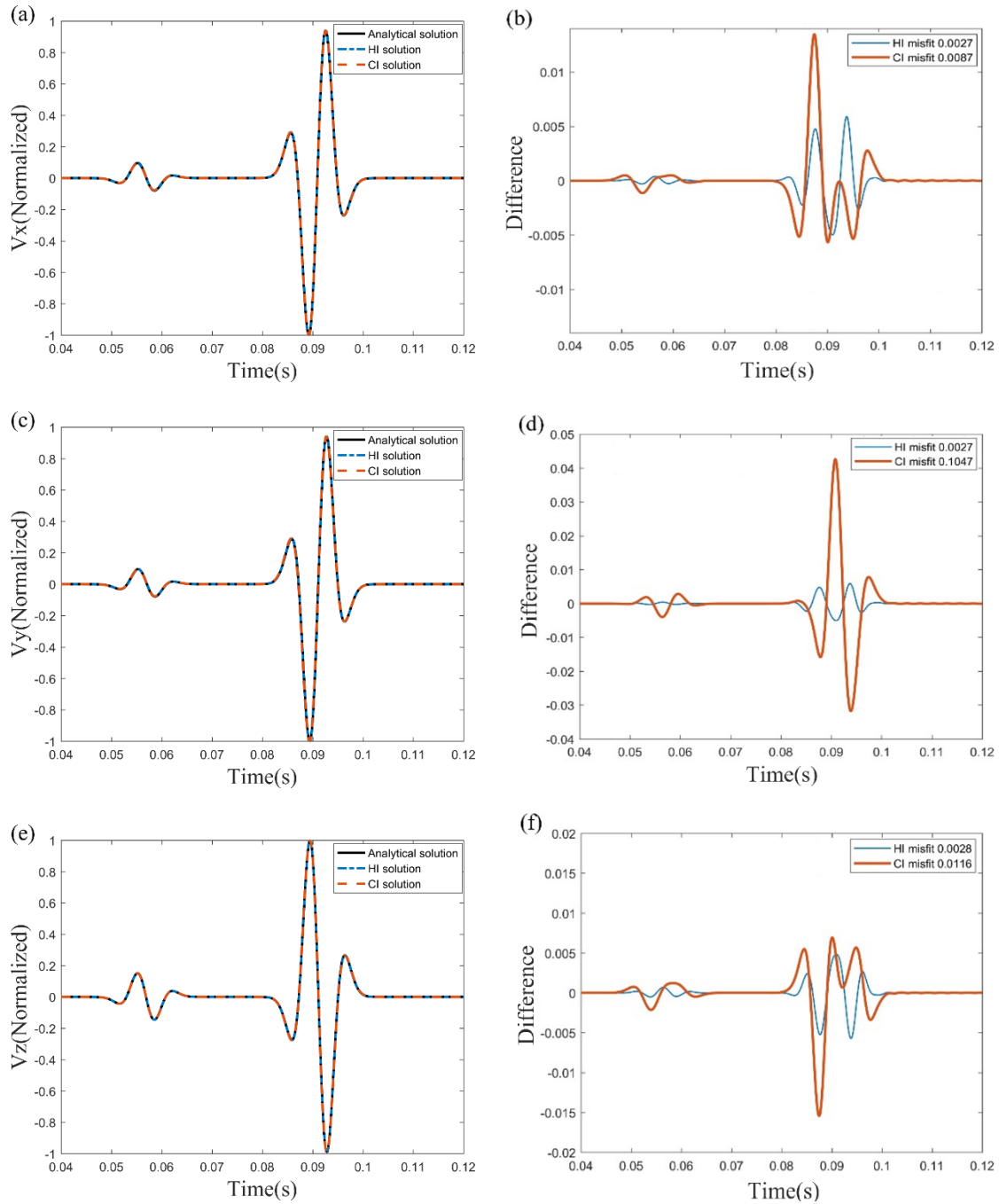


Fig. 13. The normalized velocity component obtained from two numerical solutions with 10-th order spatial discrete and analytic solution are shown in the left column, and their differences are shown in the right column. The source type is same as Fig. 12. From top to bottom is velocity component of X, Y, and Z, sequentially.

Through the simulation, the result of new improved method fits the higher order scheme perfectly, meaning it can match the analytical solution well and has higher accuracy compared with the conventional method. Especially for ISO sources, the residual wave field caused by a conventional algorithm can be significantly reduced through the simulation. For the DC and CLVD source, the numerical error is covered by the real wave and

becomes not so evident, which seems that the conventional method is on equal terms with the improved method. But the improved one has the edge on the conventional method.

It is confirmed that the improved method can be applied to more complex medium and complex focal mechanisms due to the flexibility of the finite difference method.

ACKNOWLEDGMENTS

The research was funded by Supported by the Key Research Program of Frontier Sciences, CAS (Grant No. QYZDY-SSW-DQC009) and the National Science and Technology Major Project of China (Grant No. 2017ZX05032-003-001).

REFERENCES

- Aki, K. and Richards, P.G., 2002. Quantitative Seismology, 2nd ed.. University Science Books., San Francisco.
- Baig, A. and Urbancic, T., 2010. Microseismic moment tensors: A path to understanding frac growth. *The Leading Edge*, 29, 321-323.
- Bouchon, M. (2003). A review of the discrete wavenumber method. *Pure Appl. Geophys.*, 160: 445-465.
- Burridge, R. and Knopoff, L., 1964. Body force equivalents for seismic dislocations. *Bull. Seismol. Soc. Am.*, 54: 1871-1888.
- Coutant, O., Virieux, J. and Zollo, A., 1995. Numerical source implementation in a 2D finite difference scheme for wave propagation. *Bull. Seismol. Soc. Am.*, 85, 1507-1512
- Graves, R.W., 1996. Simulating seismic wave propagation in 3D elastic media using staggered-grid finite differences. *Bull. Seismol. Soc. Am.*, 86: 1091-1106.
- Huijian, L., Runqiu, W. and Siyuan, C., 2015. Microseismic forward modeling based on different focal mechanisms used by the seismic moment tensor and elastic wave equations. *J. Geophys. Engineer.*, 12: 155-166.
- Jost, M.L. and Herrmann, R.B., 1989. A student's guide to and review of moment tensors. *Seismol. Res. Lett.*, 60, 37-57.
- Levander, A.R., 1988. Fourth-order finite-difference P-SV seismograms. *Geophysics*, 53: 1425-1436.
- Madariaga, R., 1976. Dynamics of an expanding circular fault. *Bull. Seismol. Soc. Am.*, 65: 163-182.
- Staněk, F., Eisner, L. and Moser, J.T., 2014. Stability of source mechanisms inverted from P-wave amplitude micro-seismic monitoring data acquired at the surface. *Geophys. Prosp.*, 62: 475-490.
- Virieux, J., 1984. SH wave propagation in heterogeneous media: velocity-stress finite-difference method. *Geophysics*, 49: 1933-1957.
- Virieux, J., 1986. P-SV wave propagation in heterogeneous media: velocity-stress finite-difference method. *Geophysics*, 51: 889-901.
- Yomogida, K. and Etgen, J.T., 1993. 3-D wave propagation in the Los Angeles Basin for the Whittier-Narrows earthquake. *Bull. Seismol. Soc. Am.*, 83: 1325-1342.